

---

# A Self-Calibrating, Multichannel Streak Camera for Inertial Confinement Fusion Applications

## Introduction

The OMEGA laser at LLE uses 60 symmetrically aimed laser beams to compress direct-drive inertial confinement fusion (ICF) targets.<sup>1</sup> The ICF targets are, typically, deuterium-tritium (DT)-filled microballoons. The laser beams heat and compress the target, causing the DT fuel to undergo nuclear fusion, which releases energy in the form of neutrons. The fuel must be highly compressed for this process to proceed efficiently.<sup>2</sup> The shape of the laser pulse, which typically has a length of 1 to 3 ns, can be adjusted to optimize the compression and produce a hot core of DT fuel;<sup>3</sup> however, optimal compression will happen only if the driving force imparted by the laser beams to the spherical target is uniform. If one laser beam is more energetic than its neighbors, it can seed hydrodynamic instabilities that can prevent the formation of the highly compressed core.<sup>4</sup> Because these hydrodynamic instabilities can be seeded in about 100 ps, it is necessary to ensure that the driving force imparted by the laser be uniform on the 100-ps time scale. This defines the period over which power balance must be achieved. To achieve the best target performance, the OMEGA laser must ultimately achieve 1% irradiation uniformity during each 100-ps time slice of the pulse. Achieving this goal is aided by the fact that several different beamlines illuminate any single point on the target. The averaging effect of the overlapping beams reduces the requirement for beam-to-beam power balance to 5%.<sup>5</sup>

Several factors affect power balance: In theory, if all of the optical components and all of the electrical power-conditioning units in each beamline are identical, every beamline should have the same energy and pulse shape. In practice, not all flash lamps are equal and not all optical components are equal, especially after being exposed to many shots at high optical fluences. The result is that when the laser is fired, the beams are currently energy balanced on target to 3% rms.

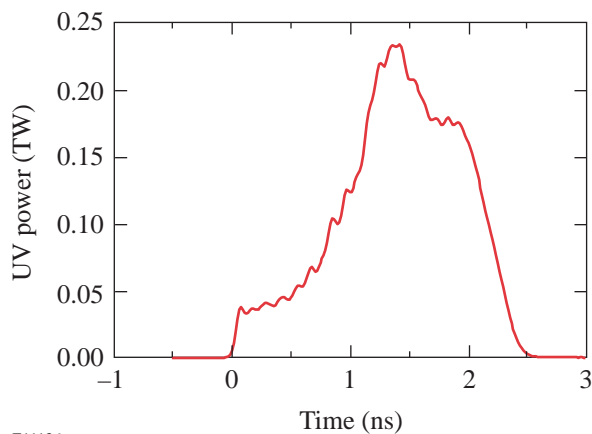
Equalizing the beam energies does not guarantee equal pulse shapes. The gains and losses of each beamline must be equal if the system is to be power balanced, which is not necessarily true for energy balance because the system is

nonlinear. For example, increasing the gain in an amplifier farther downstream can compensate for a poorly performing optic in a beamline. Although this would allow the system to be energy balanced, it will likely change the temporal shape of the optical pulse. Power balance requires that the pulse shape of all 60 beamlines be measured.

Another major factor affecting the pulse shape is the spatial-smoothing technique employed on OMEGA. Smoothing by spectral dispersion (SSD) is used to rapidly shift the speckle pattern produced at the focus of the laser.<sup>6</sup> The rapid shifting of the speckle pattern produces a uniform, time-integrated illumination profile on the ICF target. SSD works by modulating the laser frequency across the spatial and temporal profiles of the beam. Each frequency propagates at a slightly different angle with respect to the optic axis of the laser. The speckle pattern produced at the target then shifts rapidly in time. Misalignment of the SSD system, however, can cause the frequency modulation (FM) of the laser pulse to be converted into amplitude modulation (AM) at SSD drive frequencies of 3 and 10 GHz as well as at the harmonics and sum and difference frequencies. The AM can damage optical components as well as adversely affect power balance.

All of these factors can be adjusted, but only if their impact is measured. Any system that is used to measure pulse shapes on OMEGA must meet several stringent requirements. The temporal bandwidth must be able to detect temporal features in the pulse shape with frequencies as high as 10 GHz. The bandwidth is high for two reasons: First, the recorded pulse shapes are fed into theoretical models of the implosion dynamics. Higher-bandwidth signals allow more-faithful models of the implosion dynamics. Second, the 10-GHz bandwidth allows us to see any FM-to-AM conversion, which could be specific to a single beamline. The recorded signal should span a range of pulse intensities of over 1000:1. Much of the interesting implosion physics happens during the initial “foot” portion of the pulse, which is at 27% of the peak for a typical shaped optical pulse (as shown in Fig. 87.1). The recorded intensity range should be sufficient to measure the pulse shape

with an accuracy of a few percent at the peak and within about 10% in the foot. The longest pulse that can be generated with the OMEGA laser is about 4.5 ns, with 1-ns to 2-ns pulses being the most typical. The instrument record length should be slightly longer to allow us to handle the case of deliberately delayed beams, so the total record length should be about 6 ns. The OMEGA laser operates at a wavelength of 351 nm; this defines the wavelength at which the streak cameras must operate. Since there are 60 beamlines in the OMEGA system, the acquisition system must support 60 simultaneous data-acquisition channels. This data must be recorded on all OMEGA system shots, which occur on a 1-h shot cycle, so reliable operation as well as the ability to recover from equipment failure on a 1-h shot cycle is essential.

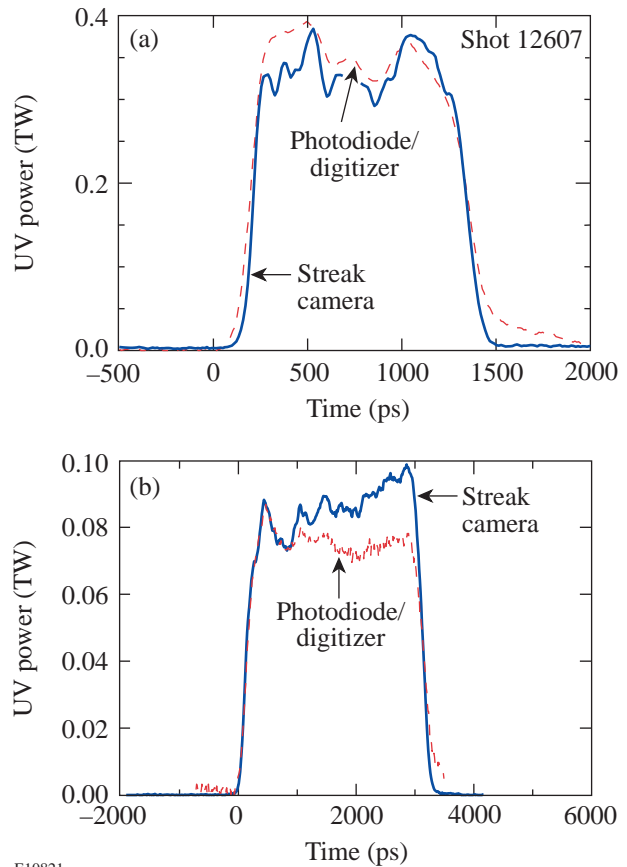


E11136

Figure 87.1

A typical shaped pulse used for ICF experiments has an initial, low-energy "foot," followed by the more-intense main part of the pulse.

Two possible alternatives were considered for a measurement system that would meet these requirements. The first alternative was to use photodiodes and transient digitizers. When the OMEGA laser was first activated, the UV pulse shape was measured with a Tektronics SCD5000 transient digitizer and a Hamamatsu photodiode. The temporal resolution of this system was about 4 GHz, which was insufficient to see the modulation due to SSD, as shown in Fig. 87.2. We have also found that photodiodes, which are optimized to measure high-bandwidth pulses, experience a droop in the signal when measuring long pulses. With a cost approaching \$70,000 per channel, this was an inappropriate option for a 60-beam laser. By way of comparison, the National Ignition Facility (NIF) at Lawrence Livermore National Laboratory is planning to monitor the 192 beams of the NIF with vacuum photodiodes and transient digitizers.<sup>7</sup> The NIF will use temporal and power multiplexing to reduce the number of digitizers and detectors



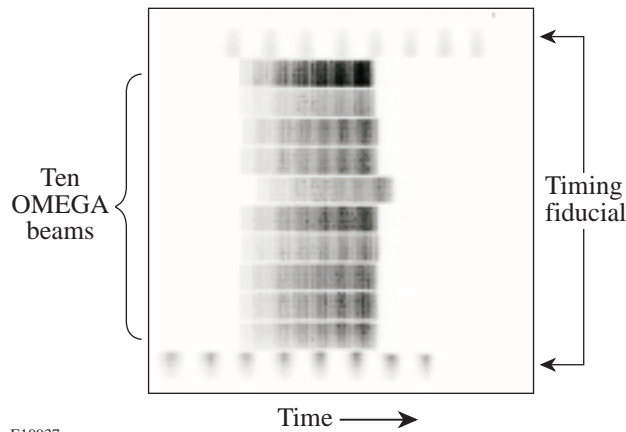
E10821

Figure 87.2

A comparison of a 4-GHz diode/digitizer to a 10-GHz streak camera. (a) The photodiode (dashed trace) was unable to reproduce the high-frequency structure measured with the streak camera (solid line). (b) One of the problems with the transient digitizer and diode measurement system (dashed trace) is a tendency for the signal to droop when measuring long pulses. This results in a distorted pulse shape as compared to the streak camera data (solid line).

to 48. The multiplexing scheme is designed to achieve a dynamic range of 5000:1 at 1 GHz with a cost per channel of \$6200. Such a system would not meet the requirements of the OMEGA laser system as stated above.

The second alternative, which is the one described in this article, uses six streak cameras to measure the UV pulses shapes in each of the 60 OMEGA beamlines. The photocathode of each streak camera is illuminated by a small portion of the light from ten OMEGA beamlines. A typical image is shown in Fig. 87.3. This system can measure all 60 beams of OMEGA with a bandwidth of 10 GHz and a per-beam dynamic range of over  $10^3$ :1. The cost per channel is about \$12,000, plus in-house labor.



E10937

Figure 87.3 The corrected image of the cluster 5 streak camera showing ten multiplexed beams and two fiducial traces. All of the beams are actually nominally co-timed. The apparent delays are due to differences in the fiber OPD to the cameras. The striations are due to FM-to-AM conversion of the 10-GHz SSD.

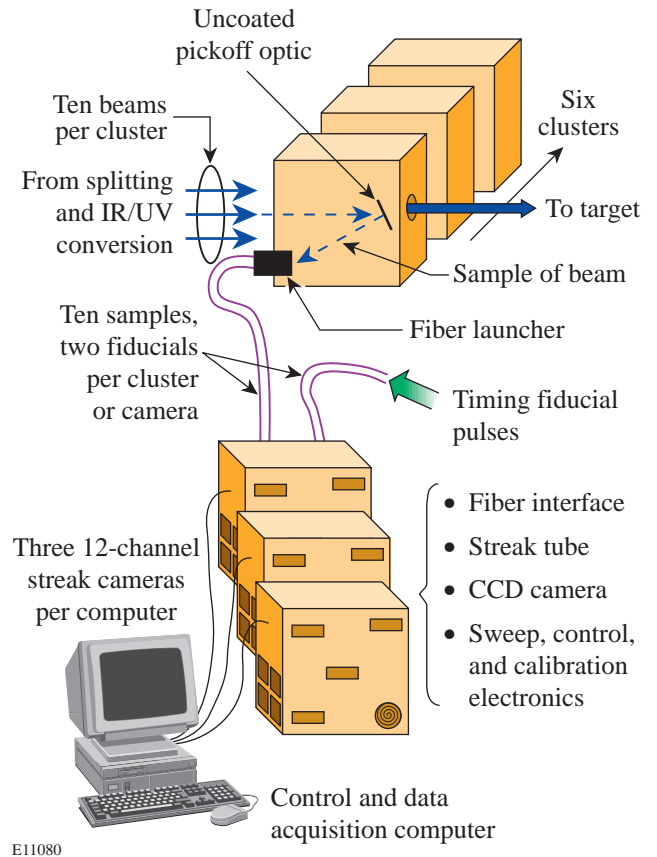
**The System**

Multichannel streak cameras are not new. A number of research groups have used them for a variety of measurements.<sup>8-10</sup> What is unique about this system is the enhanced signal-to-noise ratio (SNR) of the recorded data and the suite of autocalibration modules. These allow accurate, photometrically calibrated measurements over a period of months. OMEGA's pulse-shape-measurement system is composed of six major subsystems: the fiber launcher assembly, the optical-fiber bundles, the fiber-bundle imaging optics, the streak tube, the tube electronics, and the charge-coupled-device (CCD) camera. Each of these subsystems (illustrated in Fig. 87.4) must be optimized to meet the specifications listed above. Figure 87.5 shows the layout of the streak camera.

Each OMEGA beamline can deliver about 550 J of 351-nm light to the target. An uncoated glass surface (4% reflection) is inserted into each beam for diagnostic purposes. After three additional 4% reflections, part of the diagnostic energy is delivered to the streak camera's fiber launchers. One consequence of SSD is that each beam is about 300 times diffraction limited with an instantaneous spatial profile that has 100% speckle modulation. It is impossible to couple this light into the UV gradient-index fibers available at the time the system was constructed. The time-varying speckle coupled with angular deviation of each frequency would result in coupling losses, which would manifest themselves as AM at the output of the fiber. To overcome this problem, a system of lenses and diffusers was used to uniformly sample the spatial profile of the beam with a seven-fiber bundle. The light passes through a lens

with a 20-cm focal length, then immediately passes through a precision diffractive-optics diffuser, which spreads the light into a 2° cone angle. A second diffuser, with a 0.5° cone angle, is placed at the focus of the first lens. Finally, a 1-cm lens focuses the light into the fiber bundle. This arrangement produces a weakly modulated 2-mm-FWHM Gaussian profile at the fiber input plane at a wavelength of approximately 351 nm.

To accurately reproduce the waveform, the beam must be sampled at several points over the central portion of the 2-mm spot. The use of a 1-mm-diam-core, step index fiber would be incompatible with the required bandwidth of the system, so an alternative method was used. The 351-nm light must propagate through the 15 m of fiber from the launcher to the streak camera. The 15 m allows for equal optical path lengths from the pickoff to the camera, as well as transport through the radiation shield wall that surrounds the target chamber. To maintain the



E11080

Figure 87.4 The OMEGA pulse-shape-measurement system consists of six streak cameras, each measuring a single cluster. Optical fibers transport a small portion of the energy from each beamline to the streak cameras.

highest-possible bandwidth, a 100- $\mu\text{m}$ -core UV fiber was chosen. This high-bandwidth, UV-transmitting, graded-index optical fiber was developed by the Vavilov State Optical Institute, St. Petersburg, Russia, for use in laser diagnostics on the National Ignition Facility.<sup>11</sup> This fiber has a dispersion of 1 ps/m at 351 nm, giving a maximum bandwidth of 11 GHz. Since one fiber is inadequate to sample the entire beam, a bundle of seven fibers is used with six fibers hexagonally packed around a seventh fiber. The fiber lengths are matched such that broadening due to optical path differences (OPD's) in the bundle is negligible. To verify that the OPD's were the same, the output of a single fiber, injected with a 20-ps pulse at 351 nm, was compared with the output of a fiber bundle injected with the same pulse. The measured pulse lengths were 28 and 29 ps, respectively. The impulse response of the input fiber is therefore 21 ps, assuming the broadening and pulse width add in quadrature.

When the light emerges from the fiber bundle, it is coupled into a homogenizer bar, which produces a uniform rectangular spot from the seven-fiber hexagonal bundle by multiple surface reflections. This maximizes the fill factor on the photocathode. Ten bars are arranged in a linear array as shown in Fig. 87.6. At either end of the array are two additional homogenizer bars, which are fed by a fiducial laser operating at 527 nm. The fiducial laser is co-timed with the UV pulse from the OMEGA laser and consists of eight pulses separated by 548 ps. The fiducial pulses enable cross-timing between the six

UV streak cameras and other diagnostics in the system. An off-axis Offner triplet is used to image the optical signals onto the linear photocathode, as shown in Fig. 87.7. The mirrors are metallic, thus reducing chromatic defocus. This particular arrangement was chosen so that a variety of illumination fixtures could be placed on a computer-controlled motorized stage and individually selected to be focused onto the photocathode. The other illumination fixtures are used for *in-situ* calibration of the streak camera, which will be described later.

The streak tube is a standard commercial tube—a Philips P510—with an S-20 photocathode at the input. The electron optic terminals were biased as follows: photocathode -15 kV, slot -12.5 kV, and focus -14.5 kV. These voltages were adjusted for each tube to produce the sharpest image in the time dimension of the photocathode at the CCD with the sweep voltages held at 0 V. Figure 87.8 shows that at best focus the FWHM of the photocathode image varies as a function of both position on the photocathode and signal intensity. A low signal near the center of the image induces a broadening that has an equivalent effective bandwidth of 13.5 GHz. At the other extreme, an intense signal near the edge of the photocathode induces a broadening equivalent to 10.5 GHz. The intense signal result represents the worst possible case. The signal level was near the CCD's full well capacity. The bandwidth was limited by both saturation of the CCD and diffusive scattering in the fiber-optic coupling of the light into the CCD. This signal level is ten times what is used in normal operation.

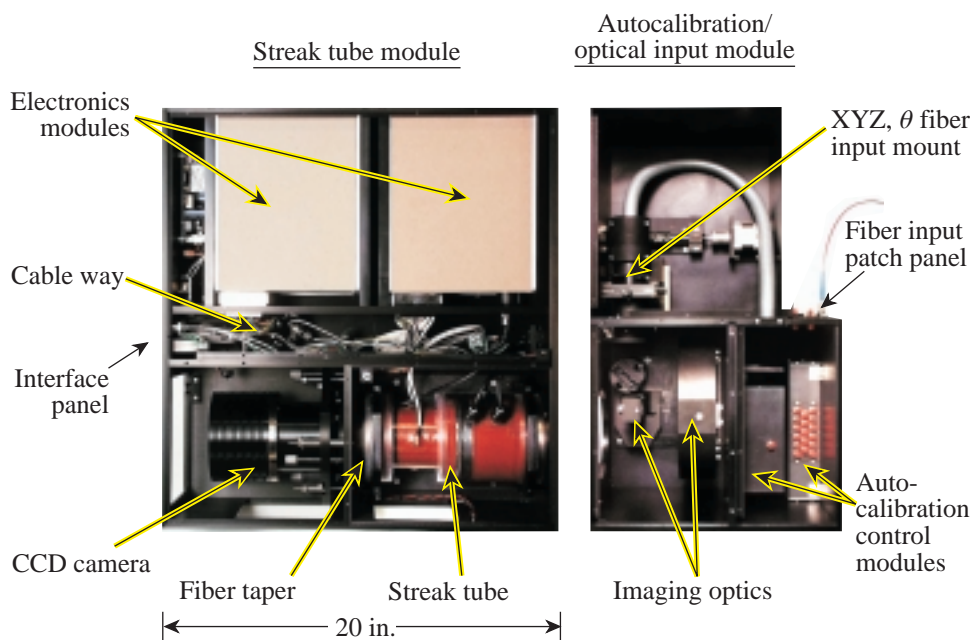
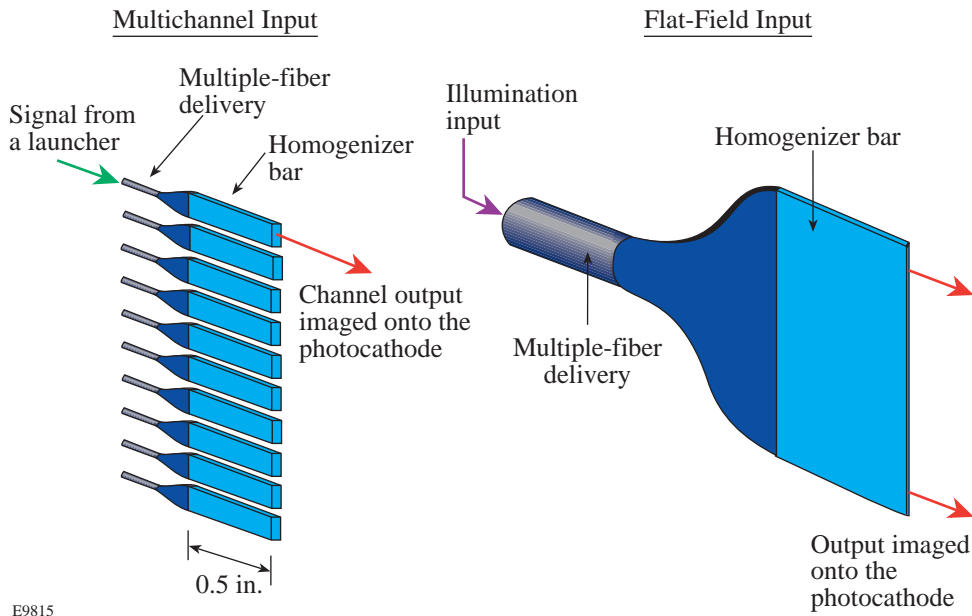
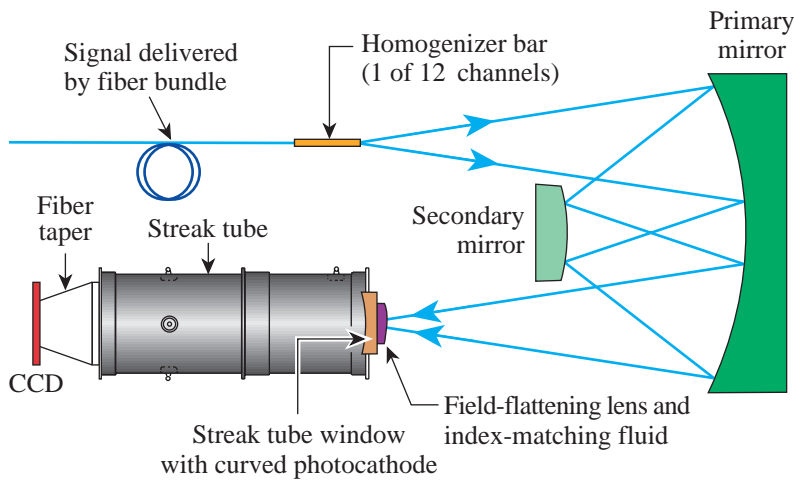


Figure 87.5  
The layout of the self-calibrating, multi-channel streak camera employed on the OMEGA laser.



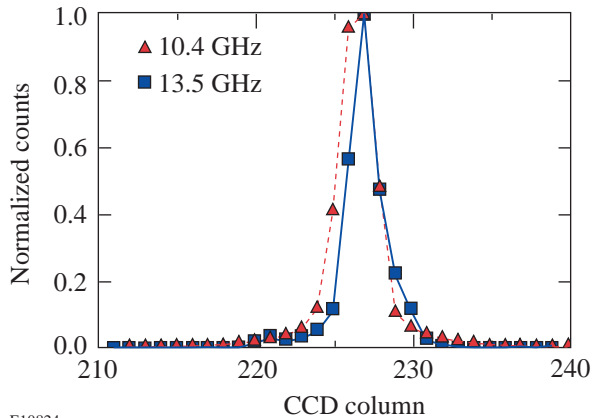
E9815

Figure 87.6  
A mechanical translation stage allows several different illumination heads to be placed at the object plane of the Offner triplet. Layouts of two illumination heads are shown here. Multiple reflections from the edges of the glass homogenizer bars produce a uniform illumination source.



E9820a

Figure 87.7  
The optical input to the streak camera uses an Offner triplet to image the fiber bundle onto the streak tube photocathode. The streak tube window is curved, and a field-flattening lens is attached to it with index-matching fluid.



E10824

Figure 87.8  
In focus mode, the image of the photocathode is adjusted to give the sharpest line at the CCD. The width of the line varies with position and intensity. The solid line shows the best focus at the center on the streak tube axis at low intensity. The FWHM is 2.5 superpixels (binned  $2 \times 2$ ) giving a bandwidth of 13.5 GHz. Off-axis and with an intense signal, the line width degrades to 3.4 pixels, corresponding to a bandwidth of 10.4 GHz.

The output fiber-optic faceplate of the tube has a P20 phosphor screen, which is reasonably well matched to the spectral sensitivity of the back-thinned CCD used to acquire the image. To match the image size at the P20 phosphor to the CCD camera, a 1.3:1 fiber-optic taper is used. Index-matching fluid is used at the mating surface between the fiber-optic taper and the streak tube to prevent the formation of Newton rings in the image recorded by the CCD camera. The CCD camera is a Roper Instruments Series 300 with a fiber-coupled  $1024 \times 1024$  CCD array using a back-thinned SITE003AB chip. There are only passive optical components between the phosphor and the CCD; no image intensifiers are used in the system. The large format of the array allows us to keep the image compression ratio of the fiber taper small, which reduces transport losses. Typically the output of this camera is binned 2 by 2 to give a  $512 \times 512$  image. This allows a rapid, low-noise readout of the array without compromising the data. At the best focus of the electron optics, the width of the photocathode image is about 2.5 superpixels wide; thus we gain no additional information by unbinning the pixels. For the remainder of this article these superpixels will be used as the standard CCD row and column unit.

The electronics for controlling the streak tubes were designed at LLE. Each camera has four interchangeable modules. The modules control the high-voltage bias, the sweep voltages, triggering, and external communications. The external communications module uses a RS-232 serial port to tell the onboard processor to read and set voltage levels, optical head positions, and sweep speeds. The high-voltage bias module sets a single high-voltage level that biases the cathode, slot, and focusing electrodes of the tube through a resistive divider. The electron optics of the tube are such that the focusing conditions are relatively insensitive to the absolute magnitude of these three voltages but very sensitive to their ratios. Thus, small variations in the power supply do not significantly affect the final image quality. In normal operation, the deflection plates of the tube are driven by a filter network, which, in turn, is driven by a MOSFET/avalanche transistor stack.<sup>12</sup> This arrangement produces a ramp that sweeps the electron beam across the phosphor screen in 6 ns and has a deviation from linearity of less than 12%. This is the standard operating sweep speed for these cameras; however, three additional sweeps of 2-ns, 20-ns, and 45-ns duration can be selected electronically. It is also possible to sweep the electron beam very slowly by ramping the voltage with a high-voltage digital-to-analog ramp. The slow ramp is used for the flat-field and geometric-distortion corrections, which are discussed in the next section.

## Calibration

The six streak cameras that measure OMEGA's 60 beams are essential to acquiring data reliably on a 1-h shot cycle. If a camera should fail, the modular design of the electronics allows us to rapidly repair the camera before the next shot. Simply acquiring data, however, is not sufficient. The data must be well calibrated and give meaningful results. *In-situ* calibration fixtures facilitate rapid recalibration of the streak cameras. It is insufficient to calibrate the streak cameras only at installation time. To ensure valid measurements at the 1% level, the streak cameras are recalibrated weekly.

A unique feature of the streak camera is the ability to slowly and uniformly ramp the electron beam across the phosphor in about 1 s. The slow ramp was designed to facilitate the acquisition of flat-field images with a large signal-to-noise ratio at very low tube currents. The slow ramp is also used to acquire images that are used to correct geometric distortions.

Several sources of geometric distortion exist in the streak camera images. The system has a set of several optic or electron-optic axes defined by the fiber-bundle array, the photocathode-electron optics, and the CCD camera. Ideally all of these axes should be aligned, but variations in tube construction cause misalignment in the electron optics. The CCD is aligned such that the image of the photocathode in focus mode (no voltage on the sweep plates) is parallel to the column axis. When voltage is applied to the streak plates, the streaked image may not move parallel to the row axis of the CCD. Fringing fields at the edges of the sweep electrodes cause pincushion distortion in the image. Also, the electron optics produce a curved image that is recorded on a flat phosphor screen. These effects must be removed from the image.

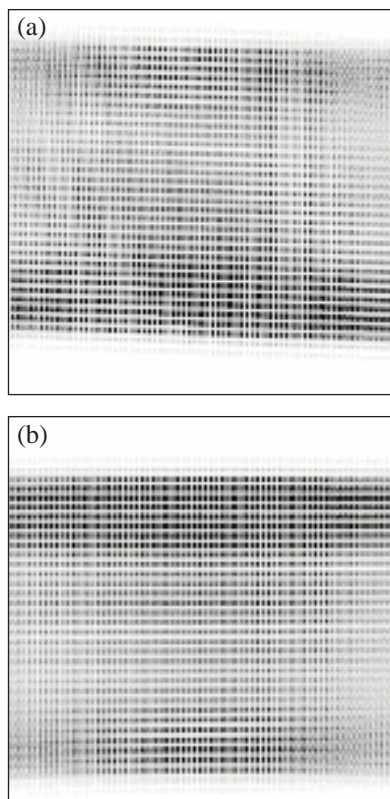
To correct these distortions, the motorized translation stage in the input optics assembly is set to the geometric distortion position. In this position, a fiber array, fed by a light-emitting diode (LED), is coupled to a homogenizer bar that uniformly illuminates the photocathode (see Fig. 87.6). A uniform wire mesh in front of the homogenizer modulates the light in the spatial direction. In this configuration, the slow ramp is used to sweep the electron beam. It takes about 1 s for the signal to sweep across the CCD. During this time, the current to the LED is modulated with a 30-Hz square wave. The resulting image consists of a uniform grid of bright rectangles (Fig. 87.9). The rectangles should be uniformly separated in space and time; however, the distortion mentioned above causes irregularities in the grid. A deconvolution algorithm is used to find the

position of each of the rectangles in the image. Next, an indexing routine assigns each rectangle its correct location in a uniform grid. The indexing of approximately 2000 points defines a mapping from the distorted to the undistorted image. Using standard image-processing techniques, the mapping can be described as an  $n$ th-order polynomial.<sup>13</sup> This procedure does not use the Jacobian of the coordinate transformation to conserve the total CCD analog-to-digital units (ADU) count. Future software upgrades will include this feature; however, when a typical geometric distortion correction is applied, the total ADU count between the corrected and uncorrected image differs by less than 0.5%, which gives acceptable results for the current implementation. Polynomial fits up to the fourth order are calculated for each mapping. The undistorted images are cross-correlated with an ideal grid to determine which polynomial degree gives the best distortion correction. The undistorted

image consists of uniformly spaced rectangles in vertical columns and horizontal rows.

Once the geometric-distortion correction has been calculated, the streak camera can be flat fielded. A traditional flat field of a CCD is insufficient because we are mapping a line to a 2-D image. Each point on the photocathode maps to a trajectory on the CCD. The geometric-distortion correction maps the trajectory of a single point on the photocathode to a single row of pixels in the undistorted image. Variations of the photocathode efficiency and the homogenizer mean that different rows are essentially illuminated with different light sources. It is important to correct the geometric distortion before correcting the flat field to guarantee that the entire row derives from the same point on the photocathode. Each pixel in a row is subjected to variations in the phosphor screen, the fiber taper, and the sensitivity of each CCD element, so the first operation in calculating the flat-field image is to normalize each pixel with respect to all the other pixels in the row. Next, the sum of the pixels in each row is normalized to all the other rows. This procedure ignores regions of the image illuminated by the edges of the photocathode where the sensitivity of the system drops down to the noise level. The flat-field illuminator is similar to the geometric-distortion fixture, but the light source is continuous and the wire grid is removed. The slow-ramp module is used to sweep the electron beam across the phosphor. In this configuration, the illumination level can be adjusted so that only a few (<10) photoelectrons are in the tube at any time during the sweep. As a result, the electron current will not distort the electric field of the focusing optics, and the signal can be collected at a larger fraction of the CCD's full well capacity than is possible in pulse mode.

Aberrations in the electron optics cause some vignetting of the electron beam at the ends of the aperture. This causes a roll-off of about 20% to 30% in the sensitivity near the edges of the sweep, as shown by the lineout of a single row (see Fig. 87.10). The slight upturn at the very edge is due to scattered photoelectrons in the tube when the beam is outside the viewing area. This creates an uncalibrated region at the edges of the tube, so trigger timing should be set to keep the signal away from the edges of the image in normal operation. The high signal levels provided by the calibration source give excellent signal to noise in the flat-field image. Additionally, the signal to noise is enhanced by averaging 120 flat-field images. These flat-field images are acquired automatically in 10 min, so the volume of calibration data greatly exceeds the volume of signal data. The slow sweep is vulnerable to stray magnetic fields at



E10829

Figure 87.9

Calibration image produced by the geometric distortion source and the slow sweep. (a) The electron optics produce a skewed and distorted image at the CCD. (b) The modulation in the distorted image is removed by a transformation that maps the image to a regular grid.

the power line frequency, which causes a ripple at the 1% level. Since the sweeps are not synchronous with the power line frequency, the ripples are averaged to zero when the 120 flat fields are averaged. In normal operation these stray fields are not a problem because their oscillation period is  $10^8$  times greater than the duration of the sweep. When the camera is operated in the fast-sweep mode, these stray fields would manifest themselves as a small, uniform dc offset in the flat field. A planned upgrade to these cameras will include the addition of  $\mu$ -metal shielding to the cameras to decrease the susceptibility to magnetic fields.

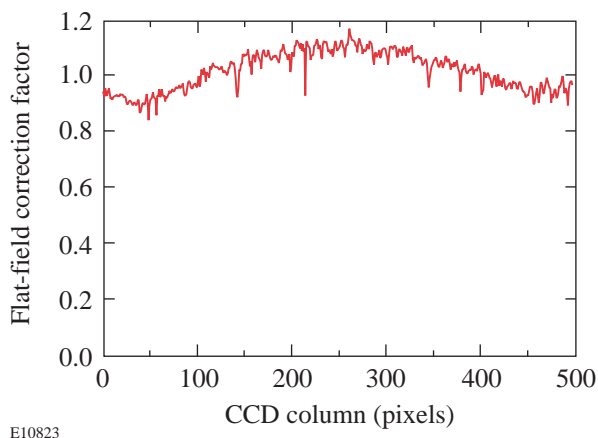


Figure 87.10

The flat-field correction factor is an image the same size as the CCD image. After geometric-distortion correction, each row in the image can be mapped to a single point on the photocathode. A lineout of one of the flat-field rows is shown. The roll-off toward the edges is due to the focusing optics obscuring part of the electron beam. The high-spatial-frequency structures are correlated with adjacent rows and are associated with dead spots in the hexagonal grid of the fiber-optic taper.

Next, the sweep speed must be calibrated. A square optical pulse is modulated with a 1.824-GHz sine wave to produce a train of eight pulses separated by 548 ps. The pulse train is injected into a fiber, and, using a 1:16 commercial fiber-optic splitter, it is divided into 12 fibers that feed a third calibration illuminator head on the streak camera. When this illuminator is placed at the object plane of the Offner triplet, the pulse train is fed to all 12 channels of the streak camera. Approximately 120 images are acquired with different trigger timing delays. The midpoint of each pulse pair in the image is assigned the derivative  $\Delta\tau$  (ps)/ $\Delta x$  (pixel), which gives about 700 independent measurements of the sweep speed for each channel distributed over the 512 pixel positions. The sweep speed cannot be calibrated at points within 274 ps of the edges. A best-fit interpolation is used to calculate  $dt/dx$ . This function is

integrated to determine time as a function of position in the CCD image. The constant of integration is chosen to assign a time of 60 ns to the center pixel. This prevents the uncalibrated region near the ends of the sweep from affecting beam-to-beam timing for all sweep speeds. The sweep speed is calculated independently for each channel. The geometric-distortion correction ensures that the sweep speed for each channel deviates from a linear fit by less than 20 ps over 5 ns, as shown in Fig. 87.11. The distortion correction should also guarantee that the sweep speeds of all the channels are identical; in practice this is not the case. Residual errors are due to uncorrected higher-order geometric distortions, resulting in slightly different sweep speeds for each channel. Finally, the sweep speed data is used to correct the recorded pixel values for the electron beam's dwell time ( $dt/dx$ ) on the pixels by dividing the recorded CCD analog to digital units (ADU) by the relative dwell time on each pixel.

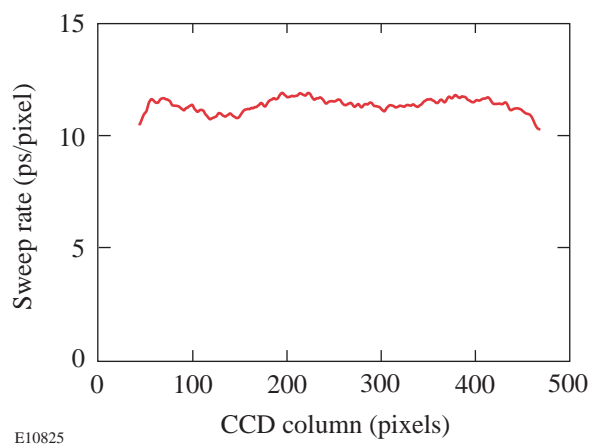


Figure 87.11

The sweep rate of a streak camera channel typically has about a 10% variation from perfect linearity. Roughly 40 channels at either end of the trace cannot be calibrated properly because of the spacing of the fiducial pulses used to calibrate the system. Most of this uncalibrated region lies in the dead zone of the flat-field image.

### Operational Considerations

Once the streak cameras are calibrated, they are approved for operation during OMEGA system shots. The calibration procedures listed above are carried out with specific voltage levels applied to the various electrodes within the streak tube. If those voltages change, the calibration is no longer valid. To guarantee that the streak cameras remain in calibration, all of the voltages applied to the streak tube are recorded at the time of the laser shot. The image acquired on the shot is stored in Hierarchical Data Format (HDF). This format allows the image, voltage settings, and background frames to be saved in

the same platform-independent computer file. We have observed that the on-shot voltages do change with time. Typically they exhibit a slow drift, which appears to be associated with the aging of components. While a feedback loop partially compensates for this drift, weekly recalibrations are still required to keep the on-shot voltage values within 1% from the average values recorded during the calibration measurements. The acceptable range is arbitrarily set at 1.5 standard deviations of the variations recorded during the calibration measurements. If more than a week elapses since the last calibration, this condition may not hold and the software will report the voltages as being out of specification.

Two positions of the motorized illumination fixture can be used to acquire streak optical data. The first illuminates the entire photocathode with the light from a single optical-fiber bundle. The second is the standard configuration, which will be discussed exclusively in the remainder of this article. The standard configuration has ten OMEGA beamlines multiplexed onto each camera along with two fiducial pulse trains, as shown in Fig. 87.3. The fiducial laser pulses serve two purposes: First, they verify the integrity of the calibration. The fiducial laser signal consists of eight pulses evenly spaced in time. On each shot, we can measure the fiducial spacing and verify that time-axis calibration is within acceptable limits. On a typical shot, the average measured period of the fiducial pulses over all six streak cameras will be 550 ps with a standard deviation of about 8 ps. The average time displacement between two binned  $2 \times 2$  superpixels is 12 ps. Thus, the timing of events with separations of the order of 0.5 ns can be determined with subpixel resolution. If, for some reason, the voltages on a streak camera go out of specification on a shot, the streak waveforms from that shot can be rescaled along the time axis by the ratio of the average fiducial period to the true fiducial period. This has been found to reduce timing errors on the distorted streak traces by 60%.

The second function of the fiducial pulse train is to determine the timing of the OMEGA beamlines. A separate instrument is used to guarantee that all beams are co-timed at target chamber center to within 10 ps. The instrument utilizes a cw mode-locked laser to check the path length of all the OMEGA beamlines and cannot operate when the main laser is fired. Data from a series of laser shots are acquired, and the timing of all the beams relative to the fiducial pulses is determined. Typically the rms timing difference between any one beam and the fiducial laser is about 15 ps averaged over 20 laser shots. Once this on-shot calibration has been completed, the streak cameras become the primary diagnostics for determining the

delay between beams and the fiducial. The OMEGA laser is often shot with some beamlines intentionally delayed. The streak cameras allow the fine adjustment of the delay. The fiducial pulse is also fed to many other target diagnostics such as x-ray streak cameras. By cross-timing with respect to the ultraviolet streak cameras, the absolute timing of any signal with respect to the laser pulse can be determined for consecutive system shots to about 10 ps rms. Over a period of several months, the jitter between the UV streak cameras and any instrument using a fiducial is less than 50 ps.

One of the primary uses of the streak cameras on OMEGA is monitoring power balance on the system, i.e., to ensure that all of the beams have the same instantaneous power.<sup>5</sup> A separate diagnostic, using a calibrated pickoff, measures the energy in each beamline to  $\pm 1\%$  precision.<sup>14</sup> The integral under the power curve measured on the streak cameras is normalized to equal the measured energy of the beamline. A plot of the streak-integrated CCD ADU versus measured UV energy is a straight line over the usable operating range of the streak cameras as shown in Fig. 87.12. This shows that not only are the streak cameras photometrically calibrated, but the response is linear over the range of typical signal levels measured on the OMEGA system. If the images show signifi-

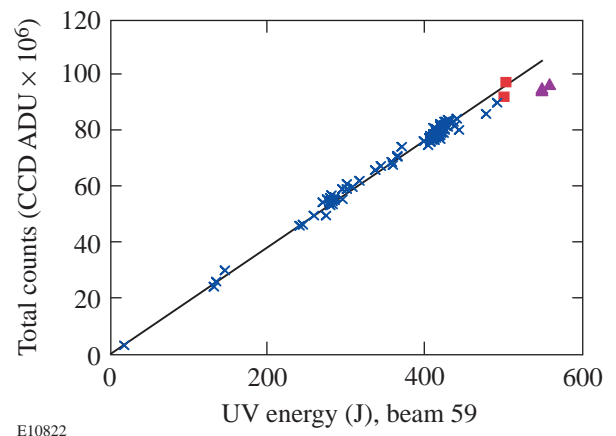


Figure 87.12 The responses of the streak cameras are photometrically calibrated. The total number of CCD counts associated with channel 59 is plotted against the measured UV energy in the beam in joules. The total number of counts is multiplied by the installed filtration. The response is linear up to 500 J UV (x's) over many different pulse shapes. The points above 500 J were 1-ns square pulses (triangles). The filtration on these shots was insufficient to prevent distortion of the streak camera image. The amount of distortion in the image depends on the number of active beams. The two points denoted by squares illustrate that the photometric calibration depends on the total streak tube current.

cant distortion, the linearity of the response breaks down, as indicated by the points designated with triangles. The ambiguity of the maximum-allowed signal level is illustrated by the two points labeled with squares at the 500-J level, which differ by about 10%. On both shots, the signal level in the channel exceeded the maximum-allowed counts. In one case, ten beams were active on the camera and the imaged was distorted. In the other case, only one beam was active for that shot and the image showed no distortion. The linearity of the sensitivity was also preserved in the latter case. Thus, it is possible for the local current density extracted from the photocathode to exceed the threshold for distortion as long as the average current density for distortion is not exceeded.

The measurable range of signal levels is determined by the optical filtration placed in front of the optical-fiber launchers. In addition to the fixed filters, two filters are on removable shuttles. These filters have attenuations of 1.75 and 5.75 and can be inserted separately or jointly, giving four possible intensity levels at the photocathode. The filtration level is chosen to get the maximum performance from the streak camera. The peak signal detected at the CCD camera is limited by the current in the electron tube. As the number of electrons in the tube increases, the image at the phosphor becomes distorted. Initially the distortion manifests itself as a spreading of the signal in both the space and time directions. As the distortion becomes more severe, the image starts to compress and bend. The maximum-acceptable level of distortion has been arbitrarily set in terms of the crosstalk between the channels in the spatial direction. When all beams on a given camera are active, the signal in the interstitial region between channels should not exceed 5% of the signal in the channel. This guarantees that the interchannel crosstalk is approximately 1% to 2% in the pixels adjacent to interchannel dead space and decays to zero in less than one-third of the channel width. Of course, this limit is flexible. If only one beam is present on a camera at a given signal level, the crosstalk distortion will be less than if all ten beams were present at the same level. The distortion is affected by both the local current density and total current in the tube. The 5% level was chosen to accept signals with 1% to 2% crosstalk between adjacent channels. At this level, the crosstalk is dominated by the decay characteristics of the streak tube phosphor and not the electron optics. Although most of the phosphorescence generated by the electron beam arrives at the CCD within a few hundred milliseconds, the phosphor will continue to emit light for as long as 10 s.<sup>9</sup> To achieve the highest optical transfer efficiency, the coupling between the CCD and the phosphor is a fiber taper. This precludes putting a shutter between the phosphor and the

CCD. Thus, as the image in the CCD shifts from row to row, it acquires an exponentially decaying tail from the phosphor decay. The last channel to be read is most affected because it has been shifted through all residual images of the other channels. We have limited this effect by choosing long exposure times, which give the phosphor time to decay before the image starts to shift, but dark current in the CCD limits exposure times. The compromise of a 3-s exposure time generates a crosstalk of 1% to 2%.

Within these limitations the useful range of the streak camera has been quantified. Each of the 12 channels is defined by 512 individual measurements. The input optics are arranged such that each channel illuminates a 24-pixel-high column on the CCD with approximately uniform intensity; thus, each of the 6144 ( $= 512 \times 12$ ) individual intensity measurements is the average of 24 individual pixel measurements. Therefore, an average, standard deviation and the signal-to-noise ratio can be calculated for each point in the waveform. Figure 87.13 shows the standard deviation plotted against the average signal for a single image on the cluster 2 camera on a log-log scale. The solid line is fit to the data at signal levels greater than the read noise of the CCD. It has a slope equal to  $0.4996 \pm 0.0574$ , which implies that the noise equals the square root of the signal times a gain factor. Thus, we are measuring a quantity that follows Poisson statistics, i.e., the photoelectrons in the streak tube. The  $x$  axis has units of CCD ADU. The dashed line is what would be expected if the streak tube photoelectrons were

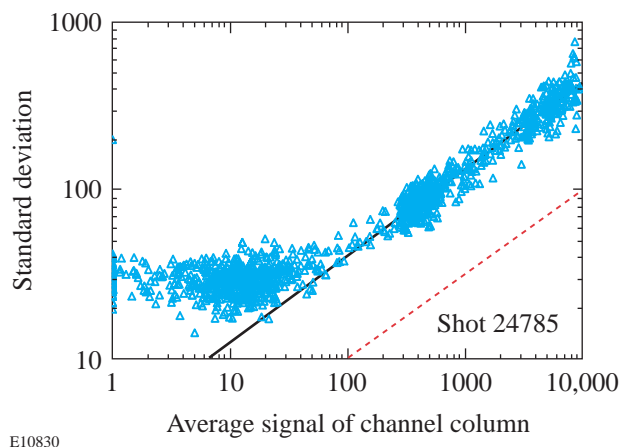


Figure 87.13

The standard deviation for  $24 \times 1$  pixel regions on the cluster 2 streak camera. At signal levels above about 30 ADU, the signal obeys Poisson statistics. Below that level, the noise is dominated by a constant read noise in the CCD electronics. The solid line is a fit of the form  $\ln(\text{std. dev}) = Ae^{[B \ln(\text{signal})]}$ , where  $B \sim 0.5$ , implying Poisson statistics. This represents the expected standard deviation if gain is removed from the system.

measured directly. The ratio or horizontal shift between the two lines is the gain of the system from streak tube photoelectrons to CCD ADU. In this case the gain is 19.2 ADU/photoelectron. In operation the optical signal was adjusted using the filters mentioned above to produce the maximum tube current that would not introduce distortion at the peak of the optical pulse. Under these conditions, the peak tube current produced 9000 CCD ADU per pixel on the cluster 2 camera. Inserting this value into the fitted equation, we find the ratio of the signal to the standard deviation at the peak to be 36. Since 24 pixels are averaged, the signal-to-noise ratio, defined as the signal times the square root of the number of averaged points divided by the standard deviation, is about 100. The signal-to-noise ratio and the peak current varied somewhat from camera to camera. The averaging time for this measurement is 12 ps. The signal-to-noise ratio drops to 1 at a signal level of 6.2 ADU.

From Fig. 87.13 the dynamic range can be estimated. At the peak, the total signal is 9000 ADU, so the dynamic range is about  $9000/6.2 = 1453$ . The noise floor is the signal level where the  $SNR = 1$  times the number of rows in a column divided by the gain, which gives a noise level of 7 photoelectrons. The noise is equivalent to about 0.3 photoelectrons per pixel. The power-balance specification for OMEGA, as well as for the NIF, requires a minimum acceptable bandwidth of 3 GHz, which corresponds to a resolution element of about 100 ps or about eight columns, so the dynamic range would increase to about  $4.1 \times 10^3$ . Quoting a dynamic range, however, is misleading. It is more important to state how the dynamic range is defined in terms of the signal-to-noise ratio. The signal-to-noise ratio is not constant over the dynamic range, and it is possible to have a very large dynamic range with a very small signal-to-noise ratio at the peak. The lower end of the dynamic range is defined as the point where the signal-to-noise ratio is equal to 1 for 12-ps averaging. At the high end of the range, tube current is just below the distortion level and the signal-to-noise ratio varies from 90:1 to 110:1. Thus at the peak of the optical pulse, measurements can be made with about 1.0% accuracy. At intensities equal to 1% and 10% of peak, the respective signal-to-noise ratios are approximately 2.3% and 7.1%. If the pulse shape being measured has regions of temporally uniform intensity, it is possible to average over longer times and get better accuracy; however, this cannot be done in regions where the pulse shape is rapidly changing in time. At the peak of this pulse the average rms error was 1.0%, which is less than the 5% error budget allotted to each beam for establishing the 1% irradiation uniformity required by OMEGA. On the rising edge, the beam timing is usually determined by the 2% threshold level. Here the signal had a 30% rms error.

Dividing the error in the power by the derivative of the power with respect to time, the error in determining the 2% point was found to be less than one CCD superpixel. These measurements show that this streak camera-based optical power measurement system is meeting the power-balance requirements of the OMEGA laser system, and in its present configuration it exceeds the specifications for the proposed NIF power-balancing system.

It is instructive to look at a single beamline to gauge how well it can be characterized. Figure 87.14 shows a beamline with a nominal, 1-ns flattop pulse with SSD. The measured pulse shape showed that both 3- and 10-GHz modulations were present. This indicated that some of the SSD bandwidth was being clipped in the amplifiers or tripling crystals. This analy-

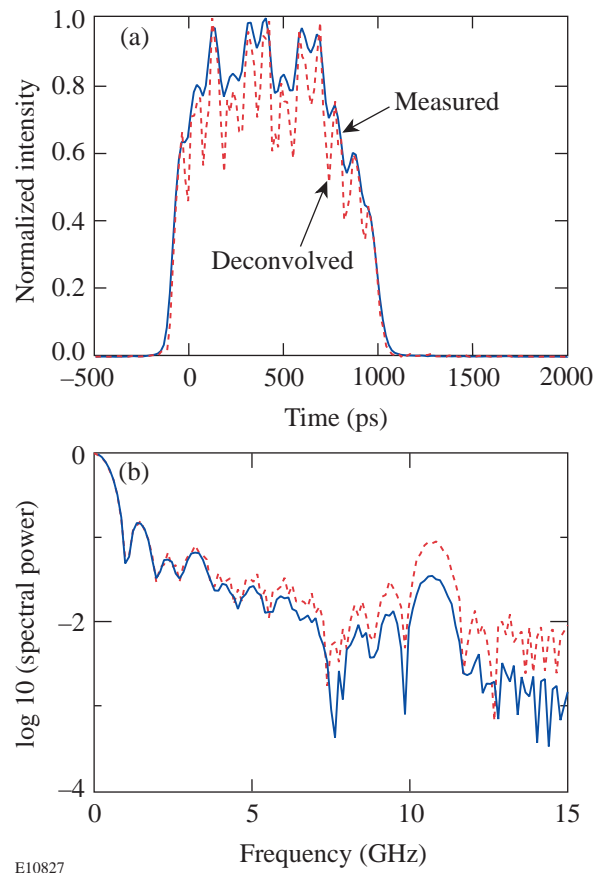


Figure 87.14 (a) The bandwidth limitation of the streak camera masks the true modulation on the pulse (solid curve). Using the measured response of the streak camera to the effects of focusing and the optical fibers, it is possible to deconvolve the bandwidth limitations (dashed curve). (b) Taking the FFT of the traces in (a), the modulation at 10 GHz is found to be three times greater in the deconvolved data than in the raw data.

sis did not take into account the bandwidth limitation of the optical-fiber bundle or the electron focusing optics discussed above. The impulse function of the camera was calculated by convolving the impulse response of the fiber bundle with the measured line spread of the focus image (see Fig. 87.8) mapped onto the sweep-speed time base. Deconvolving both of these responses from the measured signal indicated that the modulation at 10 GHz was three times higher than was being displayed.

Figure 87.15 illustrates how the streak cameras measure the power balance on the OMEGA system. The solid curve represents the normalized average pulse shape. All the beams recorded on the shot were mapped onto a uniform time base, temporally aligned, and averaged together pointwise for one of the standard OMEGA pulse shapes. The standard deviation was also calculated at each point and divided by the average, giving the dashed curve in Fig. 87.15, which is the percent of imbalance at any given time. Near the peak of the pulse, the power imbalance drops below 5%, which is the goal of the OMEGA system. The single-beam measurements indicate that the peak power of any given beamline is known with an accuracy of 1.0%. In the foot portion of the pulse, where the power is 15% to 20% of the peak, the imbalance in the system is about 10%. Here, depending on which camera is used, the single-beam measurements indicate that the power can be measured with 2% to 4% accuracy. Thus, at both the foot and the peak of this particular pulse shape, the single-beam mea-

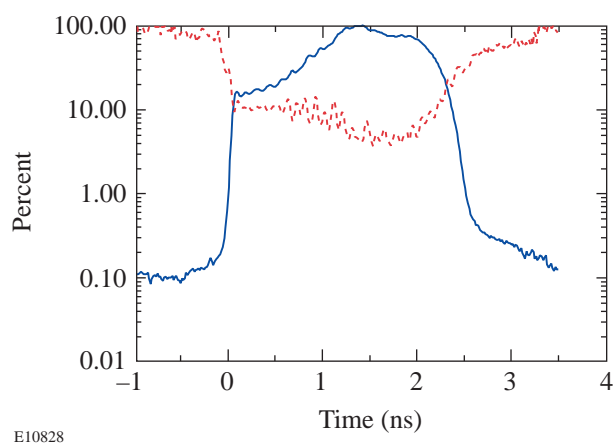


Figure 87.15

The solid curve is the average pulse shape for OMEGA shot 22708 normalized to 100% UV power at the peak averaged over 50 beams. The dashed curve is the measured standard deviation at each point across 50 beams.

surements have a smaller error than the measured beam-to-beam imbalance. As a result we have an instrument that can measure power balance on the OMEGA system and provide feedback to the engineering staff. This information can be used to modify the system, which will improve power balance. It should also be noted how well the average pulse shape of the system can be characterized. When the average shape falls to 0.1% of the peak, the average imbalance or percent error in the signal goes to 100%, implying that the SNR equals 1; thus the average pulse shape is well characterized over a 1000:1 range of powers.

## Conclusion

The design and operation of a multiplexed streak camera system have been described. The unique feature of this system is its built-in self-calibration ability. The geometric distortions, flat field, and sweep speed of each channel can be measured and adjusted on a routine basis. By maintaining a strict regime of weekly calibrations, accurate power-balance measurements on the OMEGA laser can be obtained. Over 12-ps time intervals, a single beam can be measured with 1.0% accuracy; the beam-to-beam power imbalance has been measured at less than 5%. The timing of the beams can be measured to 7-ps rms. This set of high-precision instruments is proving very useful in establishing power balance on the 60-beam OMEGA laser.

## ACKNOWLEDGMENT

This work was supported by the U.S. Department of Energy Office of Inertial Confinement Fusion under Cooperative Agreement No. DE-FC03-92SF19460, the University of Rochester, and the New York State Energy Research and Development Authority. The support of DOE does not constitute an endorsement by DOE of the views expressed in this article.

## REFERENCES

1. T. R. Boehly, R. S. Craxton, T. H. Hinterman, P. A. Jaanimagi, J. H. Kelly, T. J. Kessler, R. L. Kremens, S. A. Kumpan, S. A. Letzring, R. L. McCrory, S. F. B. Morse, W. Seka, S. Skupsky, J. M. Soures, and C. P. Verdon, *Fusion Technol.* **26**, 722 (1994).
2. J. M. Soures, R. L. McCrory, C. P. Verdon, A. Babushkin, R. E. Bahr, T. R. Boehly, R. Boni, D. K. Bradley, D. L. Brown, R. S. Craxton, J. A. Delettrez, W. R. Donaldson, R. Epstein, P. A. Jaanimagi, S. D. Jacobs, K. Kearney, R. L. Keck, J. H. Kelly, T. J. Kessler, R. L. Kremens, J. P. Knauer, S. A. Kumpan, S. A. Letzring, D. J. Lonobile, S. J. Loucks, L. D. Lund, F. J. Marshall, P. W. McKenty, D. D. Meyerhofer, S. F. B. Morse, A. Okishev, S. Papernov, G. Pien, W. Seka, R. Short, M. J. Shoup III, M. Skeldon, S. Skupsky, A. W. Schmid, D. J. Smith, S. Swales, M. Wittman, and B. Yaakobi, *Phys. Plasmas* **3**, 2108 (1996).
3. A. Okishev, M. D. Skeldon, S. A. Letzring, W. R. Donaldson, A. Babushkin, and W. Seka, in *Superintense Laser Fields*, edited by A. A. Andreev and V. M. Gordienko (SPIE, Bellingham, WA, 1996), Vol. 2770, pp. 10–17.

4. D. K. Bradley, J. A. Delettrez, R. Epstein, R. P. J. Town, C. P. Verdon, B. Yaakobi, S. Regan, F. J. Marshall, T. R. Boehly, J. P. Knauer, D. D. Meyerhofer, V. A. Smalyuk, W. Seka, D. A. Haynes, Jr., M. Gunderson, G. Junkel, C. F. Hooper, Jr., P. M. Bell, T. J. Ognibene, and R. A. Lerche, *Phys. Plasmas* **5**, 1870 (1998).
5. W. R. Donaldson, R. Boni, R. L. Keck, and P. A. Jaanimagi, in *Optical Pulse and Beam Propagation*, edited by Y. B. Band (SPIE, Bellingham, WA, 1999), Vol. 3609, pp. 121–127.
6. S. P. Regan, J. A. Marozas, J. H. Kelly, T. R. Boehly, W. R. Donaldson, P. A. Jaanimagi, R. L. Keck, T. J. Kessler, D. D. Meyerhofer, W. Seka, S. Skupsky, and V. A. Smalyuk, *J. Opt. Soc. Am. B* **17**, 1483 (2000).
7. S. W. Thomas *et al.*, in *Solid State Lasers for Applications to Inertial Confinement Fusion: Second Annual International Conference*, edited by M. L. Andre (SPIE, Bellingham, WA, 1997), Vol. 3047, pp. 700–706.
8. J. Chang *et al.*, in *Digest of Technical Papers, Fifth IEEE Pulsed Power Conference*, edited by P. J. Turchi and M. F. Rose (IEEE, New York, 1985), pp. 1–4.
9. R. A. Lerche, D. S. Montgomery, and J. D. Wiedwald, in *Ultrahigh- and High-Speed Photography, Videography, and Photonics '91*, edited by P. A. Jaanimagi (SPIE, Bellingham, WA, 1992), Vol. 1539, pp. 68–75.
10. G. A. Kyrala *et al.*, *Rev. Sci. Instrum.* **68**, 664 (1997).
11. A. V. Okishev, R. Boni, M. Millecchia, P. A. Jaanimagi, W. R. Donaldson, R. L. Keck, W. Seka, K. V. Dukelsky, M. A. Eronyan, V. S. Shevandin, G. A. Ermolaeva, G. Nikolaev, and V. B. Shilov, “Unique High-Bandwidth, UV Fiber Delivery System for the OMEGA Diagnostic Applications,” to be published in the *IEEE Journal on Selected Topics in Quantum Electronics*.
12. Laboratory for Laser Energetics LLE Review **73**, 6, NTIS document No. DOE/SF/19460-212 (1997). Copies may be obtained from the National Technical Information Service, Springfield, VA 22161.
13. E. L. Hall, *Computer Image Processing and Recognition*, Computer Science and Applied Mathematics (Academic Press, New York, 1979), pp. 186–188.
14. Laboratory for Laser Energetics LLE Review **63**, 110, NTIS document No. DOE/SF/19460-91 (1995). Copies may be obtained from the National Technical Information Service, Springfield, VA 22161.